JACS ARTICLES

Published on Web 05/21/2010

Molecular Spintronics in Mixed-Valence Magnetic Dimers: The Double-Exchange Blockade Mechanism

Alessandro Soncini,*,† Talal Mallah,‡ and Liviu F. Chibotaru†

Institute for Nanoscale Physics and Chemistry (INPAC) and Division of Quantum and Physical Chemistry, Katholieke Universiteit Leuven, Celestijnenlaan 200F, B-3001 Heverlee, Belgium, and Institut de Chimie Moléculaire et des Matériaux d'Orsay, Université Paris Sud 11, Rue George Clemenceau, 91405 Orsay, France

Received March 5, 2010; E-mail: Alessandro.Soncini@chem.kuleuven.be

Abstract: We theoretically investigate the charge and spin transport through a binuclear $Fe^{III}Fe^{III}$ iron complex connected to two metallic electrodes. During the transport process, the $Fe^{III}Fe^{III}$ dimer undergoes a one-electron reduction (Coulomb blockade transport regime), leading to the reduced mixed-valence $Fe^{II}Fe^{III}$ species. For such a system, the additional electron may be fully delocalized leading to the stabilization of the highest spin ground state $S = 9/2$ by the double exchange mechanism, while the original $Fe^{III}Fe^{III}$ has usually an $S = 0$ spin ground state due to the antiferromagnetic exchange coupling between the two Fe^{III} ions. Intuitively, the spin delocalization within the mixed-valence complex may be thought to favor charge and spin transport through the molecule between the two metallic electrodes. Contrary to such an intuitive concept, we find that the increased delocalization leads in fact to a blocking of the transport, if the exchange coupling interaction within the $Fe^{III}Fe^{III}$ dimer is antiferromagnetic. This is due to the violation of the spin angular momentum conservation, where a change of half a unit of spin ($\Delta S = 1/2$) is allowed between two different redox states of the molecule. The result is explained in terms of a *double-exchange blockade* mechanism, triggered by the interplay between spin delocalization and antiferromagnetic coupling between the magnetic cores. Consequently, ferromagnetically coupled dimers are shown not to be affected by the double-exchange blockade mechanism. The situation is evocative of the onset and removal of giant magnetoresistance in the conductance of diamagnetic layers, as a function of the relative alignment of the magnetization of two weakly antiferromagnetically coupled ferromagnetic contacts. Numerical simulations accounting for the effect of vibronic coupling show that the spin current increases as a function of spin delocalization in Class I and Class II mixed-valence dimers. The signature of vibronic coupling on sequential spin-tunneling processes through Class I and Class II mixed-valence systems is identified and discussed.

Introduction

The ambitious quest for the ultimate miniaturization of electronic devices has fostered a very intense research activity on molecular electronics and spintronics.[1] Molecular nanomagnets represent a particularly fertile ground for nanospintronics, as it is expected that the possibility of controlling the slow dynamics of their magnetization via spin currents could have ground-breaking applications in the very promising quest for molecular spin qubits for quantum computation.[2] Pioneering electron transport experiments performed on a cobalt complex,[3] on a vanadium dimer,[4] Mn_{12}ac,[5] and a single Mn^{2+} ion complex[6] have clearly shown that electron transport through molecular nanomagnets provides a probe for strong electron correlation effects, which leads to phenomena such as the Coulomb blockade, cotunneling, and Kondo resonance.

† Katholieke Universiteit Leuven.
‡ Université Paris Sud 11.

(1) Nitzan, A.; Ratner, M. A. *Science* **2003**, *300*, 1384. Rocha, A.; García-Suárez, V. M.; Bailey, S. W.; Lambert, C. J.; Ferrer, J.; Sanvito, S. *Nat. Mater.* **2005**, *4*, 335. Bogani, L.; Wernsdorfer, W. *Nat. Mater.* **2008**, *7*, 179. Giusti, A.; Charron, G.; Mazerat, S.; Compain, J.-D.; Mialane, P.; Dolbecq, A.; Riviére, E.; Wernsdorfer, W.; Biboum, R. N.; Keita, B.; Nadjo, L.; Filoramo, A.; Bourgoin, J.-P.; Mallah, T. *Angew. Chem., Int. Ed.* **2009**, *48*, 4949. Mannini, M.; Pineider, F.; Sainctavit, P.; Danieli, C.; Otero, E.; Sciancalepore, C.; Talarico, A. M.; Arrio, M.-A.; Cornia, A.; Gatteschi, D.; Sessoli, R. *Nat. Mater.* **2009**, *8*, 194. Gambardella, P.; Stepanow, S.; Dmitriev, A.; Honolka, J.; de Groot, F. M. F.; Lingenfelder, M.; Sen Gupta, S.; Sarma, D. D.; Bencok, P.; Stanescu, S.; Clair, S.; Pons, S.; Lin, N.; Seitsonen, A. P.; Brune, H.; Barth, J. V.; Kern, K. *Nat. Mater.* **2009**, *8*, 189.

(2) Timco, G. A.; Carretta, S.; Troiani, F.; Tuna, F.; Pritchard, R. J.; Muryn, C. A.; McInnes, E. J. L.; Ghirri, A.; Candini, A.; Santini, P.; Amoretti, G.; Affronte, M.; Winpenny, R. E. P. *Nat. Nanotechnol.* **2009**, *4*, 173.

(3) Park, J.; Pasupathy, A. N.; Goldsmith, J. I.; Chang, C.; Yaish, Y.; Petta, J. R.; Rinkoski, M.; Sethna, J. P.; Abruna, H. D.; McEuen, P. L.; Ralph, D. C. *Nature* **2002**, *417*, 722.

(4) Liang, W.; Shores, M. P.; Bockrath, M.; Long, J. R.; Park, H. *Nature* **2002**, *417*, 725.

(5) Heersche, H. B.; de Groot, Z.; Folk, J. A.; van der Zant, H. S. J.; Romeike, C.; Wegewijs, M. R.; Zobbi, L.; Barreca, D.; Tondello, E.; Cornia, A. *Phys. Rev. Lett.* **2006**, *96*, 206801. Jo, M.-H.; Grose, J. E.; Baheti, K.; Deshmukh, M. M.; Sokol, J. J.; Rumberger, E. M.; Hendrickson, D. N.; Long, J. R.; Park, H.; Ralph, D. C. *Nano Lett.* **2006**, *6*, 2014.

(6) Osorio, E. A.; Moth-Poulsen, K.; van der Zant, H. S. J.; Paaske, J.; Hedegård, P; Flensberg, K.; Bendix, J.; Bjørnholm, T. *Nano Lett.* **2009**, *10*, 105.

 10.1021/ja101887f

One class of binuclear transition metal complexes that has been proposed as particularly promising for molecular conduction consists of mixed-valence molecular wires, i.e. typically Ru(II)Ru(III) mixed-valence dimers, where the two metals with formally different oxidation states, are linked by π-conjugated spacers.[7−9] Mixed-valence compounds allowing for long-range intramolecular electron transfer are thus advocated as potentially efficient systems for the expanding domain of nanojunctions.[8,9] A natural generalization of mixed-valence molecular wires emerges by considering mixed-valence dimers with a magnetic core. Such systems could in fact provide excellent candidates for molecular spintronics, since, in addition to the efficient intercenter electron transfer, they provide additional magnetic degrees of freedom that can be manipulated via spin currents.

The primary goal of this work is to investigate mixed-valence Fe(II)Fe(III) magnetic dimers as devices for molecular spintronics. Fe(II)Fe(III) dimers have the same number of valence *d*-electrons as Ru(II)Ru(III) dimers and share their tendency to delocalize the excess electron. However, the multielectronic states of Fe(II)Fe(III) mixed-valence dimers are markedly different from those of Ru(II)Ru(III), mainly because the electronic structure of the local ions is described by high-spin configurations, which lead to exchange-coupled "magnetic cores" in the dimer structure. Thus, as we will briefly review later in this work, the energetics of the final electronic states for mixed-valent Fe(II)Fe(III) dimers is strongly dependent on the interplay between exchange coupling between magnetic cores and the extent of excess-electron transfer between the iron cores. A well-known example of a highly delocalized mixed-valence iron dimer, representing one of the systems that are the focus of this work, is the compound[10] $[Fe_2(OH)_3(tmtacn)_2]^{2+}$ (tmtacn = *N*′,*N*″,*N*‴-trimethyl-1,4,7-triazacyclononane), whose structure is represented in Figure 1, within an idealized setting for a molecular device.

Although several theoretical studies have already appeared in the literature describing spin transport of weakly anisotropic magnetic molecules,[11−14] interestingly, all previous works have systematically neglected the mixed-valence character of the reduced states resulting from the charging process. Reduced states have in fact been described solely in terms of a Hund rule type interaction between the spin of the injected electron and the total spin of the oxidized exchange states. In other words, the effects of direct chemical bonding between neighboring metal ions, leading to strong intramolecular charge-transfer effects of the itinerant electron, have always been neglected. The first description of intramolecular charge transfer effects on spin transport of magnetic molecules has been introduced in a recent work by two of the present authors.[15] However, in that work only strongly anisotropic noncollinear magnetic molecules were investigated, in which exchange coupling between magnetic centers represents only a small perturbation.

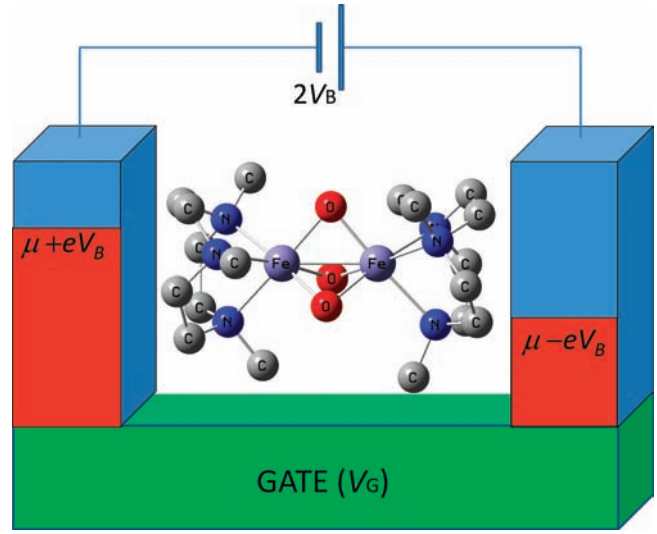

Figure 1. Idealized scheme of a typical molecular device considered in this work, consisting of an Fe(II)Fe(III) mixed valence iron dimer, in the picture represented by the class III mixed-valence iron dimer $[Fe_2(OH)_3(tmtacn)_2]^{2+}$ compound (hydrogen nuclei not shown), connected to two metal electrodes (blue rods) kept at different chemical potentials by an applied bias voltage V_B (the occupied energy leveles in the electrodes are represented by a red shaded area). The structure is ideally deposited on an insulating layer (green base) kept at a fixed potential V_G, which provides the source of an additional static electric field or gate voltage, which can be used to tune the energy gaps between the states of the neutral and the charged species (see text for additional details).

Thus, the effect of intramolecular charge transfer on spin transport through strongly exchange-coupled (and weakly anisotropic) systems such as mixed-valence complexes remains to date unexplored and represents the focus of this work.

Spin-delocalization effects in mixed-valence systems are described by the double-exchange mechanism, within the model introduced by Anderson and Hasegawa,[16] and subsequently rationalized in exchange-coupled magnetic molecules by Girerd[17] and others.[18−22] Mixed-valence systems are traditionally classified by the extent of delocalization of the additional electron, ranging from complete localization (Class I) to complete delocalization (Class III).[23] Thus $[Fe_2(OH)_3(tmtacn)_2]^{2+}$ is a well-known example of a Class III mixed valent system, whereas the $[Fe_2S_2]^+$, the core iron dimer of e.g. the reduced $[Fe_2S_2](S\text{-}Cys)_4$ complex (Cys = cysteinyl ligands) present in reduced Fe_2S_2 ferredoxin proteins,[24] is a well-known example of a Class II mixed valence system with a magnetic core.[10] Imidazolate-bridged divanadium complexes, mixed-valence systems with a magnetic core, have been recently characterized as fully delocalized Class III compounds with a high-spin ground state.[25]

As extensively described in the chemical and physical literature,[16−22] the characterizing trait of mixed-valence systems

(7) Creutz, C.; Taube, H. *J. Am. Chem. Soc.* **1973**, *95*, 1086.
(8) Fraysse, S.; Coudret, C.; Launay, J-.P. *J. Am. Chem. Soc.* **2003**, *125*, 5880.
(9) Fabre, M.; Bonvoisin, J. *J. Am. Chem. Soc.* **2007**, *129*, 1434.
(10) Gamelin, D. R.; Bominaar, E. L.; Kirk, M. L.; Wieghardt, K.; Solomon, E. I. *J. Am. Chem. Soc.* **1996**, *118*, 8085. Gamelin, D. R.; Bominaar, E. L.; Mathoniere, C.; Kirk, M. L.; Wieghardt, K.; Girerd, J.-J.; Solomon, E. I. *Inorg. Chem.* **1996**, *35*, 4323.
(11) Elste, F.; Timm, C. *Phys. Rev. B* **2005**, *71*, 155403.
(12) Romeike, C.; Wegewijs, M. R.; Hofstetter, W; Schoeller, H. *Phys. Rev. Lett.* **2006**, *96*, 196601.
(13) Gonzales, G.; Leuenberger, M. N. *Phys. Rev. Lett.* **2007**, *98*, 256804.
(14) Misiorny, M.; Barnas, J. *Phys. Status Solidi B* **2009**, *246*, 695.
(15) Soncini, A.; Chibotaru, L. F. *Phys. Rev. B* **2010**, *81*, 132403.
(16) Anderson, P. W.; Hasegawa, H. *Phys. Rev.* **1955**, *100*, 675.
(17) Girerd, J.-J. *J. Chem. Phys.* **1983**, *79*, 1766.
(18) Belinskii, M. I.; Tsukerblat, B. S.; Gerbeleu, N. V. *Sov. Phys. Solid State* **1983**, *79*, 497.
(19) Noodelman, L.; Baerends, E. J. *J. Chem. Phys.* **1984**, *106*, 2316.
(20) Borshch, S. A.; Kotov, I. N.; Bersuker, I. B. *Sov. J. Chem. Phys.* **1985**, *3*, 1009.
(21) Yoo, J.; Yamaguchi, A.; Nakano, M.; Krzystek, J.; Streib, W. E.; Brunel, L. C.; Ishimoto, H.; Christou, G.; Hendrickson, D. N. *Inorg. Chem.* **2001**, *40*, 4604.
(22) Guihéry, N.; Malrieu, J. P. *J. Chem. Phys.* **2003**, *119*, 8956.
(23) Robin, M. B.; Day, P. *Adv. Inorg. Chem. Radiochem.* **1967**, *10*, 247.
(24) Bertini, I.; Ciurli, S.; Luchinat, C. *Struct. Bonding (Berlin, Ger.)* **1995**, *83*, 1.

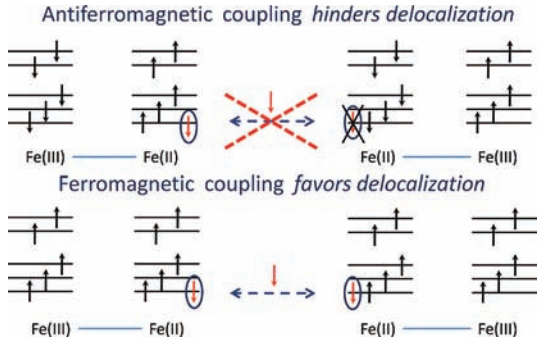

Figure 2. Illustration of the double exchange mechanism: interplay between the delocalization tendency of the charge transfer process between the two iron ions, favored by ferromagnetic coupling between magnetic cores, and the localization tendency of antiferromagnetic coupling between the magnetic Fe(III) cores. The electron occupation of the valence *d*-shell orbitals for the two iron ions in the dimer is illustrated for the Fe(II) and Fe(III) oxidation states involved in the double-exchange process, assuming locally quasi-octahedral ligand fields. Resonance between different valence configurations is indicated by dashed double arrows. The excess electron responsible for spin-delocalization is encircled (red). Top: Antiferromagnetic coupling leads to antiparallel alignment of the magnetic Fe(III) cores, which, in turn, hinders delocalization of the excess electron, due to unfavorable Hund-rule coupling between the excess electron and the local magnetic core. Bottom: Ferromagnetic coupling between the Fe(III) cores, on the other hand, favors electron delocalization via the double-exchange mechanism.

such as Ru(II)Ru(III) and Fe(II)Fe(III) dimers consists of the delocalized character of the excess electron, to a greater or lesser extent, between the two metal ions. Whereas in Ru(II)Ru(III) systems the extent of delocalization is strongly mediated by the coupling between ions and bridging ligands, in Fe(II)Fe(III) dimers delocalization mechanisms can be more direct, involving direct metal−metal bonding.[17] If the metal centers of the oxidized dimer precursor of the mixed-valent species are magnetic ions coupled antiferromagnetically, such as in the Fe(III)Fe(III) oxidized species considered in this work, the chemical bonding of the mixed-valence dimer obtained upon reduction cannot be described solely in terms of the excess electron delocalization. In fact, as mentioned above, bonding will be the result of the interplay between two competing mechanisms: (i) the electron transfer between iron cores via a direct metal−metal bond, which tends to delocalize the excess electron, and (ii) the antiferromagnetic exchange coupling between the magnetic cores, which tends to localize the excess electron on one of the two metal ions. Thus, as illustrated in Figure 2 and further detailed in the next section, the electron transfer process between the two magnetic ions can couple two equivalent antiferromagnetically coupled configurations: Fe(II)Fe(III) and Fe(III)Fe(II). For very weak electron transfer rates, the spectrum consists of two almost identical copies of the Heisenberg exchange coupled spectrum characterizing the two equivalent configurations, slightly split by the electron transfer process. The doubling of Heisenberg exchange energy levels caused by intramolecular charge transfer represents the reason why the process is named "double exchange".[17]

The origin of the two competing delocalization and localization processes, at the heart of the double-exchange mechanism, and unique to mixed-valent systems *with a magnetic core*, are illustrated in Figure 2, where the relevant octahedral *d*-orbital configurations for Fe(II)Fe(III) dimers are considered. In systems with strong metal−metal bonds (class III), such as the $[Fe_2(OH)_3(tmtacn)_2]^{2+}$ dimer reported in Figure 1, the delocalization tendency of the double exchange mechanism prevails over the antiferromagnetic exchange coupling, which dominates in the oxidized dimer Fe(III)Fe(III), leading to a spin-unpairing process upon reduction: the *antiferromagnetic* Fe(III)Fe(III) dimer turns into the *ferromagnetic* Fe(II)Fe(III) mixed-valence system upon charging, to favor spin delocalization.

On a purely intuitive level, one would expect Class III mixed-valence magnetic molecules to serve as excellent intermediate reduced states in spintronics conduction processes, by virtue of the fact that sequential spin tunneling is mediated by states in which the "itinerant spin" is fully delocalized over all magnetic centers. Here we show that in fact the spin current is completely blocked when the reduced magnet is a Class III compound. Moreover, the conditions whereby the vibronic states of Class I and Class II mixed-valence systems can serve as optimal intermediate states in the sequential spin-tunneling transport process are identified and discussed.

Redox States and Coulomb Blockade Transport

Transport experiments on magnetic molecules in break-junctions setups have shown that the most relevant transport regime is Coulomb blockade (CB).[3−5]

The Coulomb blockade transport regime is a noncoherent transport regime that occurs in molecular devices in which the coupling between the molecule and the metal contacts is relatively weak. This condition is often realized in metal complexes: even if it is in principle possible to design ligands capable of binding the electrodes quite strongly, the ligand−metal bonds are usually relatively weak, so that the effective coupling between the metal sites on the molecule, and the electrodes, is often quite small. In this case, the journey of the itinerant electron between the source and the drain electrodes is relatively slow, so that the transmission of the electron from source to drain contacts occurs via an intermediate process, namely, the reduction of the molecular complex.

The CB conduction process thus occurs in two steps. First the occupied states on the source electrode exchange one electron with the *N*-electron molecule and give rise to an $N+1$-electron reduced species. Second, the reduced complex exchanges one electron with the empty states on the drain electrode, thus returning into an oxidized state, and transmitting the electron current to the drain. This two-step tunneling process is also named *sequential tunneling*, since tunneling from source to drain can only occur as a sequence of one-electron charging (step one) and discharging (step two) processes. In order for the full two-step tunneling process to occur and a nonzero current to be measured at the drain electrode, the difference between the chemical potential of the oxidized *N*-electron species and the chemical potential of the reduced $N+1$-electron complex must be smaller than, roughly, the applied bias voltage V_B (see Figure 3). In other words, the energy provided by the external voltage must be sufficient for the intermediate reduction process to occur. However, in metal complexes the charging energy is typically quite large due to electron repulsion on the metal sites, so that the chemical potential of the reduced complex typically lies too high above that of the oxidized species for the itinerant electron to carry out the reduction (see Figure 3, on the left). The impossibility of charging the complex due to large Coulomb repulsion between the itinerant electron and the electrons making up chemical bonds on the molecular device leads to a blockage of the tunneling process, representing the

(25) Bechlars, B.; D'Alessandro, D. M.; Jenkins, D. M.; Iavarone, A. T.; Glover, S. D.; Kubiak, C. P.; Long, J. R. *Nat. Chem.* **2010**, *2*, 362.

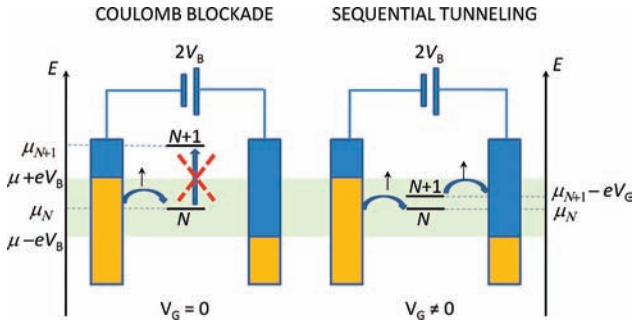

Figure 3. Illustration of the Coulomb blockade mechanism and its "unblockage" via an applied gate voltage (V_G). Two energy schemes are shown (left and right), each representing the different components (two electrodes and one molecule) of a molecular device. The electrodes are represented by a continuum of energy levels. The occupied levels are shaded in a lighter color (yellow); the empty levels are shaded in a darker color (blue). The border between the lighter and darker shadings in the electrodes represents the quasi-equilibrium chemical potential of that electrode, kept higher (lower) in the source (drain) electrode by the applied bias voltage (V_B). Tunneling conduction processes can occur only via molecular states whose energy lies within the conduction window, the energy region highlighted via a light shading (green) horizontally crossing the diagram. The chemical potentials associated with the N-electron oxidized (μ_N) and the $N + 1$-electron reduced (μ_{N+1}) molecular complexes are represented by discrete energy levels. Although both oxidized and reduced chemical potentials can vary as a function of V_G, the state with higher charge ($N + 1$) will vary faster, and for some value of V_G the two states will be in resonance. Assuming that both chemical potentials vary linearly with the gate field, we plot here only the gap between the two redox states, setting μ_N as an effective zero, for ease of visualization. Left: In the Coulomb blockade regime the chemical potential of the reduced molecular species lies outside the conduction window; thus the itinerant electron does not have enough energy to change the redox state of the N-electron molecule, and the conduction is blocked. Right: An external electric field (gate voltage) lowers the chemical potential of the $N + 1$-reduced chemical species, favoring the reduction process and, eventually, setting a sequential tunneling current in the molecular device.

essence of the Coulomb blockade mechanism. The application of an external electric field (the gate voltage V_G) can stabilize the charged states, making the reduction process less energetically expensive (i.e., lowering the chemical potential of the reduced species; see Figure 3, on the right), thus removing the Coulomb charging barrier and giving rise to a sequential tunneling current.

In this work we consider a molecular device setup which consists of two electrodes kept at different chemical potentials by an external bias voltage (V_B), coupled to an Fe(III)−Fe(III) dimer (see Figure 1). An additional gate voltage is applied (V_G). To simulate CB transport it is necessary to have a model for the different redox states of the molecular device, which will be created by electron injection from the source and electron withdrawal from the drain. Neglecting the effects of spin−orbit coupling, the lowest lying states of the noncharged nanomagnet with n unpaired electrons well localized on N metal centers with local spin s are well described by the Heisenberg exchange Hamiltonian:

$$\mathrm{H}_n = -J \sum_{\langle ij \rangle} \mathbf{s}_i \cdot \mathbf{s}_j \qquad (1)$$

where J is the exchange coupling constant between nearest neighbors.

In previous studies on spin transport through exchange-coupled polynuclear complexes, the states of the reduced magnetic molecule have always been approximated by exchange coupled states formed by coupling the spin states of the oxidized system with the spin of the additional electron. Effects related to the occupancy of local d-orbitals on single metal centers by the additional electron, and the effect of hopping processes between metal cores, have only been considered for strongly anisotropic magnetic molecules.[15]

However, fundamental features characterizing the electronic structure of mixed valence compounds, such as spin localization or delocalization, described by the interplay between superexchange, double-exchange, and vibronic coupling mechanisms, are intrinsically rooted in the hopping process of the additional electron between metal centers.

Consequently, the following model Hamiltonian for the reduced magnetic states is considered here:[15]

$$\mathrm{H}_{n+Q} = \mathrm{H}_n + (\varepsilon - eQV_G) \sum_{p}^{N} \sum_{\sigma}^{\uparrow\downarrow} n_{p\sigma} + \beta \sum_{\langle pq \rangle} \sum_{\sigma}^{\uparrow\downarrow} c_{p\sigma}^{\dagger} c_{q\sigma} + U \sum_{p}^{N} n_{p\uparrow} n_{p\downarrow} + J_{\mathrm{H}} \sum_{p}^{N} \sum_{\alpha}^{\uparrow\downarrow} \sum_{\beta}^{\uparrow\downarrow} \mathbf{s}_p \cdot \boldsymbol{\sigma}_{p,\alpha\beta} c_{p\alpha}^{\dagger} c_{p\beta}, \qquad (2)$$

where ε is the energy of a set of spin−orbitals *localized* on the metal sites (e.g., the metal d orbitals), $c_{p\sigma}^{\dagger}$ are creation operators for the on-site spin−orbitals, $n_{p\sigma} = c_{p\sigma}^{\dagger} c_{p\sigma}$, β is a hopping parameter between centers, U is the Coulomb repulsion between two electrons on the same center, σ_p are Pauli matrices associated to an electronic spin injected on site p, and J_H is the Hund's rule coupling between the spin of the excess electron on site p and the spin moment $\mathbf{s}_p$ on that center ($J_H < 0$). Here we confine ourselves within the region around the first CB diamond, where only singly charged states are relevant together with the neutral ones. This is formally achieved by setting $U \rightarrow \infty$.

Further simplification of the Hamiltonian eq 2 occurs by analyzing the detailed electronic structure change in the Fe(III) → Fe (II) reduction process. The electronic structure of the oxidized Fe(III) ion is described by a high spin term ($s = 5/2$), in which the crystal-field split d-orbitals are all occupied by a single electron. Regardless of the crystal field around the iron ions (typically a trigonal distortion of a perfect octahedral environment) and the resulting splitting pattern of the d-orbital manifold, the injected electron during the transport process will occupy a semioccupied orbital in the d-shell, pairing up its spin with the electron occupying the lowest lying d-orbital (or degenerate manifold; see Figure 2). By virtue of the Hund's coupling rule, described by the last term in the Hamiltonian eq 2, the four remaining unpaired d-electrons give rise to a high-spin electronic ground term, corresponding to on-site spin $s = 2$. Thus, to describe charging processes occurring at low bias and gate voltages, we can consider only those singly charged mixed-valence states resulting from the interplay of the Heisenberg antiferromagnetic exchange coupling between two sets of on-site electronic terms with fixed spins (one with $s = 2$, the other with $s = 5/2$), interchanged by a one-electron transfer process.

These are very well-known states.[17] Let us name $|SM(A)\rangle$ ($S = 1/2, 3/2, ..., 9/2$), the spin states of the exchange-coupled Fe(II)Fe(III) configuration, and $|SM(B)\rangle$, the exchange spin states of the configuration Fe(III)Fe(II). The simplest representation of the mixed valence states is thus obtained by taking the bonding and antibonding combinations of $|SM(A)\rangle$ and $|SM(B)\rangle$.

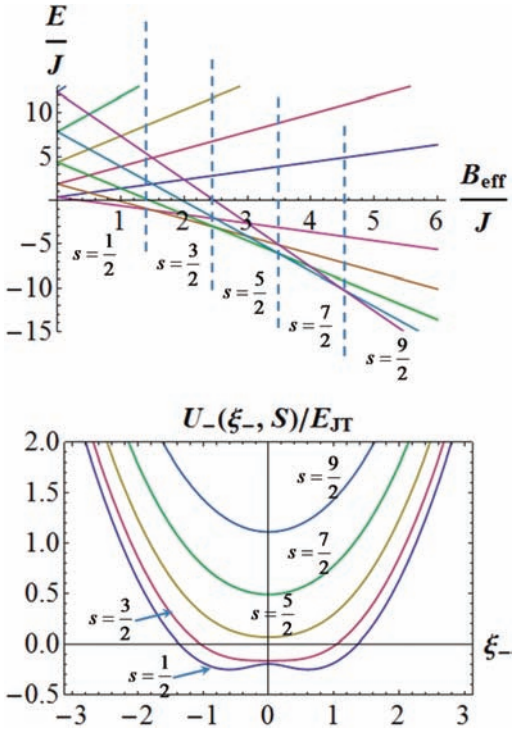

Figure 4. Top: Energy spectrum of an antiferromagnetic Fe(II)Fe(III) mixed-valence dimer as function of the effective double-exchange parameter. The total spin of the ground state is indicated, and spin transitions occurring in the ground state as a function of B_{eff} are indicated by dashed vertical lines. Bottom: Adiabatic potential energy curves for the spin states of a typical antiferromagnetic Fe(II)Fe(III) Class II mixed-valence dimer. The antiferromagnetic exchange parameter J, double-exchange parameter B_{eff}, and the vibronic stabilization energy $E_{\text{JT}} \equiv \lambda_-^2/k_-$ are the experimental values[10] reproducing the spectrum of the Class II mixed-valence dimer $[Fe_2S_2]^+$: $J = -360\ \text{cm}^{-1}$, $B_{\text{eff}} = -965\ \text{cm}^{-1}$, $\lambda_-^2/k_- = 3660\ \text{cm}^{-1}$.

The resulting spectrum is described by the well-known expression[17]

$$E_{n+1}^{\pm}(S) = -\frac{J}{2}S(S+1) \pm B_{\text{eff}}\left(S+\frac{1}{2}\right) \tag{3}$$

where the + (−) sign refers to symmetric (antisymmetric) combinations and $B_{\text{eff}} = \beta/(2s_0 + 1)$ is the effective coupling constant for the intercenter electron-transfer process ($s_0 = 5/2$). The behavior of the energy spectrum described by eq 3 as a function of B_{eff}/J is reported at the top of Figure 4. For large β (i.e., direct metal−metal bond), the symmetric combination of $S = 9/2$ high-spin states gains enough delocalization energy to become the 10-fold degenerate ferromagnetic ground state. On the other hand, if exchange coupling J is the dominant energy scale, the resulting spectrum consists of two almost-degenerate copies of the usual Heisenberg spin ladder spectrum, where each spin rung is weakly split by the electron transfer interaction. When β is small ($B_{\text{eff}}/J < <1$), the ground and first excited manifolds of the Fe(II)Fe(III) mixed-valence compound are both doublets (see Figure 4).

To describe the extent of localization or delocalization of the charging electron over the two Fe-centers for different values of β/J, it is also necessary to take into account symmetry breaking processes associated with vibronic coupling. Vibronic coupling arises in mixed valence systems from the fact that when the additional electron is localized on the first iron center, giving rise to the collective spin state $|SM(A)\rangle$, the local spin state on center A (the one with lower spin $s_A = 2$) makes the local breathing mode q_A stiffer than the same breathing mode q_B localized on center B (with higher local spin $s_B = 5/2$). The converse is true when the electron is localized in $|SM(B)\rangle$. It can thus be shown that the normal mode $q_- = 2^{-1/2}(q_A - q_B)$ leads to a transfer assisted vibronic coupling mechanism between the $|SM(A)\rangle$ and $|SM(B)\rangle$ spin states.[26] Let the elastic constant for the mode q_- be k_- and the vibronic coupling constant be λ_-. The vibronic problem written on the basis of the symmetric/antisymmetric superposition of the states $|SM(A)\rangle$ and $|SM(B)\rangle$ reads[27]

$$H_{n+1}(q_-, S) = \frac{k_-}{2}q_-^2 + \begin{pmatrix} B_{\text{eff}}\left(S+\frac{1}{2}\right) & \frac{\lambda_-}{\sqrt{2}}q_- \\ \frac{\lambda_-}{\sqrt{2}}q_- & -B_{\text{eff}}\left(S+\frac{1}{2}\right) \end{pmatrix} \tag{4}$$

In the adiabatic limit, the spin-dependent potential energy curves are easily obtained by diagonalization of eq 4 and can be written as functions of the dimensionless vibrational coordinate $\xi_- = q_-/(\lambda_-/k_-)$ as

$$U_{n+1}^{\pm}(\xi_-, S) = -\frac{J}{2}S(S+1) + \frac{1}{2}\left(\frac{\lambda_-^2}{k_-}\right)\xi_-^2 \pm \sqrt{\frac{1}{2}\left(\frac{\lambda_-^2}{k_-}\right)^2\xi_-^2 + B_{\text{eff}}^2\left(S+\frac{1}{2}\right)^2} \tag{5}$$

The propensity of the charging electron to valence trapping is related to the ratio $B_{\text{eff}}(S + {}^1/_2)/(\lambda_-^2/k_-)$ in the potential curves (eq 5). From eq 5 it is in fact clear that large electron transfer rates imply that the ground state is described by a high-spin adiabatic potential similar to a parabolic potential with the minimum at $\xi_- = 0$ (Class III systems), whereas small hopping rates lead to an instability in the low-spin ground state potential, resulting in a double-well potential with two displaced minima, as illustrated in Figure 4 (Class II and Class I systems).[17,28]

To introduce dynamical effects in the vibronic coupling problem for the reduced states, especially important in the weak electron-transfer limit, we adopt here the "diabatic" approach. In other words, we first find the states of Hamiltonian eq 4 neglecting at first electron-transfer processes. The resulting electronic states are the original $|SM(A)\rangle$ and $|SM(B)\rangle$, and the energies provide harmonic potentials for two displaced harmonic oscillators with energy minima at $\xi_-^A = -\lambda_-/k_-$ and $\xi_-^B = +\lambda_-/k_-$. Thus we can write the vibronic basis as

$$|A, n\rangle = |SM(A)\rangle\chi_n(\xi - \xi_-^A),\ |B, n'\rangle = |SM(B)\rangle\chi_{n'}(\xi - \xi_-^B)$$
$$n, n' = 0, 1, 2, ..., N_{vib} \tag{6}$$

where $\chi_n(\xi - \xi_-^i)$ are the harmonic oscillator eigenfunctions centered at ξ_-^i with quantum number n. The final vibronic states

(26) Piepho, S. B.; Krausz, E. R.; Schatz, P. N. *J. Am. Chem. Soc.* **1978**, *100*, 2996.
(27) Blondin, G.; Girerd, J.-J. *Chem. Rev.* **1990**, *90*, 1359.
(28) In the class I mixed-valent compounds, according to the Robin and Day classification, the two metal sites belong to different chemical elements. Therefore the model in eq 2 should include a parameter describing the difference of the orbital energies on the two metal sites for the itinerant electron; also the parameters U and J_H should be taken differently for the two metal sites. We note, however, that by varying the bias voltage we can bring the orbital energies on the metal sites in resonance, thus reducing effectively the class I compound to the class II one.

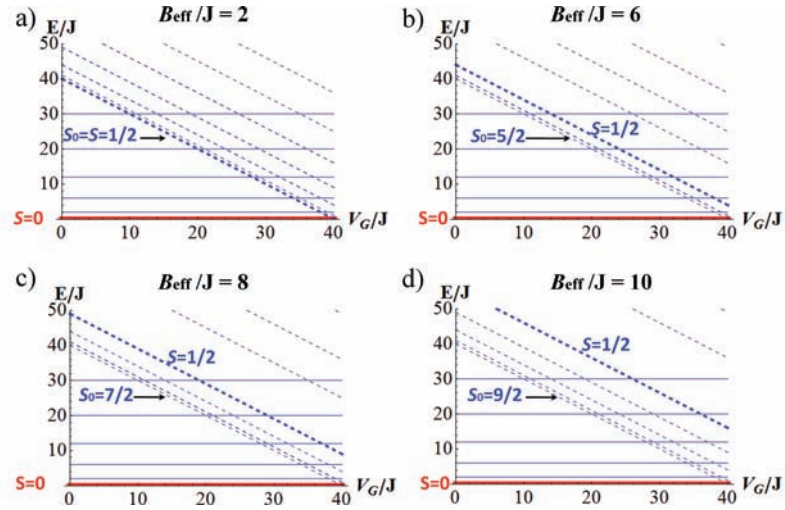

Figure 5. Dependence of the energy gap between the electronic states of neutral (solid lines) and singly charged (dashed lines) iron dimer on the applied gate voltage (V_G), for different extents of electron transfer: (a) $B_{eff}/J = 2$, (b) $B_{eff}/J = 6$, (c) $B_{eff}/J = 8$, (d) $B_{eff}/J = 10$. Sequential tunneling conductance can be observed only when the $S = 0$ and $S = 1/2$ states are brought to resonance by the external gate voltage, as in the subfigure (a). The $S = 1/2$ energy level is indicated with a dashed bold line. S_0 labels the spin of the ground state of the charged dimer. It is assumed here that, for $V_G = 0$, the gap between the ground states of neutral and charged species is equal to $40J$ (if $J \approx 200$ cm^{-1}, the gap is $\sim$1 eV). This implies that the minimal gate voltage necessary to bring to resonance the ground states of neutral and charged species is $V_G = 40J$. Note that, only in the weak transfer limit ($B_{eff}/J = 2$), $V_G = 40J$ is sufficient to remove the Coulomb blockade regime.

are obtained by diagonalizing the electron-hopping Hamiltonian on the basis of eq 6, choosing $N_{vib} + 1$ vibrational states for each of the two noninteracting displaced harmonic wells. The vibronic matrix is reported in eq 1 of the Supporting Information. Once the vibronic wave functions for the redox states are determined, the Coulomb-blockade transport problem can be easily set up and solved. The relevant details of the methodology followed in this work for the calculation of the charge and spin currents are reported in the Supporting Information.

Results and Discussion

In the CB regime, an applied bias voltage alone cannot cause any current flow, since the states of the reduced species lie higher in energy with respect to the states of the oxidized species (see Figure 3, left side). To remove the blockade, an additional source of energy must be provided, via an external electric field (gate voltage, see Figure 3, right side), which should match at least the lowest energy gap between the states of the oxidized and reduced species (see Figure 5). Thus, given that generally iron dimers are antiferromagnetically coupled, the Fe(III)Fe(III) → Fe (II)Fe(III) charging process will couple the singlet ground state of the antiferromagnetic Fe(III)Fe(III) dimer and the ground state of the mixed valence system Fe(II)Fe(III).

It follows that different values of B_{eff}/J can lead to qualitatively different charging processes. In fact, as it is shown in Figures 5 and 6, for any value of B_{eff}/J, the ground state of the Fe(III)Fe(III) dimer always remains a singlet, while that of the mixed-valence Fe(III)Fe(II) dimer varies from 1/2 to 9/2 depending on B_{eff}/J. As a consequence, as a function of B_{eff}/J, four spin transitions can occur, and five different mixed-valent ground states will be formed upon charging (see also top of Figure 4). As illustrated in Figure 5, assuming without loss of generality that the ground state of the mixed-valent dimer is separated in energy from the $S = 0$ ground state of Fe(III)Fe(III) by a gap of $40J$, it will be necessary to apply a gate voltage $V_G = 40J$ to remove the Coulomb blockade and observe a (spin) tunneling current. However, the total spin of the mixed-valence state that is in resonance with the $S = 0$ state when the gate

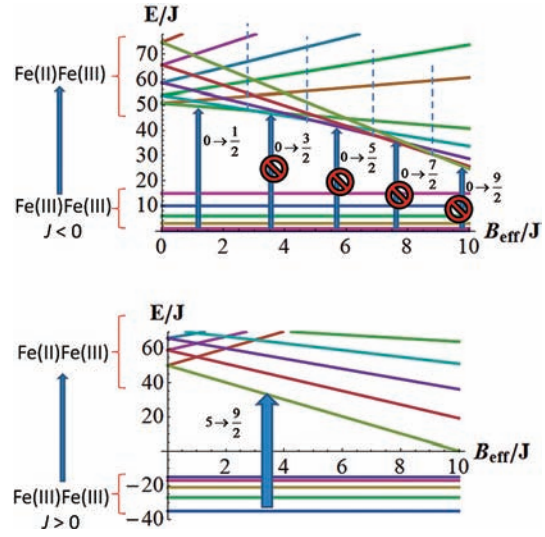

Figure 6. Dependence on the extent of electron transfer (B_{eff}/J) of the lowest lying charging-process for an antiferromagnetic (top) and a ferromagnetic (bottom) Fe(III)Fe(III) dimer. The blue arrows indicate the lowest energy charging process mechanism. The red "forbidden signs" in the top portion indicate spin-angular mometum forbidden charging processes for an antiferromagnetic dimer beyond some threshold value of B_{eff}/J, representing the double-exchange spin-blockade mechanism (see text).

voltage $V_G = 40J$ is applied will be strongly dependent on the extent of electron delocalization in the mixed-valent system: thus if $B_{eff}/J \approx 2$, the charged mixed-valent state $S = 1/2$ will be in resonance with the neutral $S = 0$ (see Figure 5 a), whereas if $B_{eff}/J \approx 8$, then at $V_G = 40J$ the resonance will occur between the charged $S = 7/2$ Fe(II)Fe(III) ground state and the $S = 0$ neutral Fe(III)Fe(III) ground state (see Figure 5 c). In the latter case, the current will be carried by the $S = 7/2$ mixed-valent state, whereas in the former case it will be carried by the $S = 1/2$ mixed-valent state.

However, any one-electron reduction process responsible for CB sequential tunneling transport can only change the ground state spin angular momentum of the oxidized species by half a

unit, as it is also evident from the matrix elements determining the transition rates in eqs 3 of the Supporting Information. Thus, within the sequential tunneling transport process, *it is only possible to reduce the Fe(III)Fe(III) singlet ground state if* B_{eff}/J *is small enough to allow a mixed-valence* $S = 1/2$ *ground state*, which is only for Class I and certain Class II systems. In the example illustrated in Figure 5, only in the first case (Figure 5a) at $V_G = 40J$ it will be possible to measure a tunneling current, whereas in the other three cases the system will *remain in a blockade regime* and no current will be measured.

In other words, if the ground state of the mixed-valence dimer has undergone spin transition (i.e., if $S = 1/2$ is not the ground state anymore), the charging one-electron process with the lowest energy cost becomes forbidden (see top of Figure 6). Hence, the matrix elements defining the transition rates reported in eq 3 of the Supporting Information are identically zero, no population transfer between the oxidized and reduced species is allowed to occur even if enough energy is provided by the gate voltage, and ultimately, no current can flow through the molecular device.

We define here the mechanism underlying this blocked sequential tunneling regime the *double-exchange blockade mechanism* (see top of Figure 6). Note that in Class III systems the double-exchange blockade mechanism will be equally active for α and β electrons and for any value of the spin polarization of the ferromagnetic source. Thus, not only the spin current but also the charge current, sum of α and β spin-polarized currents, will be completely blocked in Class III mixed-valence systems. We note that the recently reported experimental observation of spin-blockade phenomena in the sequential tunneling conductance spectrum of a Mn^{2+} *mononuclear* complex[6] is not related to the mechanism hereby described, being rooted in a spin transition induced by the external gate voltage. On the other hand, the double-exchange (spin and charge) blockade can be expected to occur only in *polynuclear* complexes, by virtue of the interplay beteween antiferromagnetic superexchange and spin delocalization.

The scenario is completely different if the exchange coupling interaction is ferromagnetic in the oxidized species. In this case, both ground states of the oxidized and reduced species are described by high-spin states ($S = 5$ for the oxidized, and $S = 9/2$ for the reduced system), their spin angular momenta differing only by half a unit ($\Delta S = 1/2$) for any value of B_{eff}/J (see bottom of Figure 6). Under these relatively rare circumstances, the molecular device will always work as a sequential-tunneling conductor, under a gate voltage bringing the oxidized $S = 5$ and the reduced $S = 9/2$ ground states into resonance. This radically different behavior of ferromagnetic and antiferromagnetic Class III compounds is evocative of the giant magnetoresistance effect in diamagnetic layers sandwiched between two ferromaganetic electrodes that are weakly antiferromagnetically coupled. Thus, as antiferromagnetic coupling in class III mixed valence dimers quenches charge and spin sequential tunneling currents, so the onset of giant magnetoresistance is observed in diamagnetic channels for antiparallel alignment of the weakly antiferromagnetically coupled ferromagnetic electrodes. On the other hand, as the giant magnetoresistance effect ceases to exist when the ferromagnetic electrodes are driven parallel by a weak external magnetic field, similarly, the double-exchange blockade is removed in ferromagnetic mixed-valence dimers.

Clearly, beyond these similarities, there exist important differences between the two phenomena, mainly due to the fact that giant magnetoresistance is triggered by the relative orientation of two blocked thermodynamic magnetic phases, whereas ferromagnetic and antiferromagnetic coupling in iron dimers is due to coherent microscopic coupling mechanisms of electrostatic origin, resulting in isotropic time-reversal symmetric quantum spin states. Accordingly, giant magnetoresistance is a purely magnetic effect differentiating between electrons with opposite spin polarizations. As such, it can only be relevant for spin currents. On the contrary, the double-exchange blockade mechanism results from quantum interference between the wave function of the additional injected electron hopping between magnetic centers and the ferromagnetic or antiferromagnetic quantum spin states of a single molecule. If the coupling is antiferromagnetic, the ground state of the mixed-valence system that undergoes spin transition as a function of spin delocalization will be unaccessible to the itinerant electron coupled to the oxidized singlet state, regardless of the spin polarization of the tunneling electron. The double exchange blockade will thus be active not only for spin currents but also for charge currents. These conclusions are very general and are independent of the effect of vibronic coupling. Clearly, higher order mechanisms can be active nevertheless, such as cotunneling.[14] However, for weak electrode-molecule coupling, these effects are orders of magnitude smaller than sequential tunneling currents and will be neglected in the present work.

On the other hand, vibronic effects become crucial to investigate spin transport through localized (Class I and II) mixed-valence systems. Here we simulate sequential spin-tunneling conduction in Fe(III)Fe(III) dimers, including in our calculations only the singlet and triplet states for the neutral species as well as the two doublets and two quartets describing the mixed-valence lowest lying spectrum in the weak delocalization limit. We assume in our simulation that the source electrode is fully spin polarized ($\nu_L^{\uparrow} = 1$ in eqs 3 of the Supporting Information) and the drain is nonmagnetic ($\nu_R^{\uparrow} = \nu_R^{\downarrow} = 1/2$ in eqs 3 of the Supporting Information). For convenience, we fix the parameters related to the vibrational and vibronic problem to typical experimental values for the $[Fe_2S_2]^+$ Class II complex core[10] ($\hbar\omega_{vib} = 310\ cm^{-1}$ for the vibrational quantum, the reduced mass $\mu = 32\ g\ mol^{-1}$, the vibronic energy $\lambda_-^2/k_- = 3660\ cm^{-1}$).

After a systematic investigation of the effect of increasing the vibrational basis set on the eigenvectors and eigenvalues of the vibronic matrix (see eq 1) of the Supporting Information, we find that the minimal basis capable to reproduce all vibronic features of the Coulomb blockade spin-transport $I-V$ diagram consists of 12 harmonic oscillator states (6 for each of the 2 displaced potential wells) for each spin state. The results of the calculations are shown in Figure 7. The spin current as a function of B_{eff}/J (J is chosen here to be of the same order as the vibrational quantum $\hbar\omega_{vib}$) displays two discontinuities, thus identifying three distinct spin-transport regimes (Figure 7a). For small B_{eff}/J, the current grows nonlinearly as a function of the delocalization extent. At $B_{eff}/J \approx 1.7$ the spin current experiences a discontinuity, suddenly dropping to less than half its magnitude. For $B_{eff}/J > 1.7$ the spin current magnitude starts to grow again, up to $B_{eff}/J \approx 2.3$, when it suddenly drops to zero. Thus, given $|J| \approx \hbar\omega_{vib}$, the prediction is that for $B_{eff}/J > 2.3$ the spin current will be completely suppressed, despite the growing delocalization extent of the reduced mixed-valence states.

The behavior of the spin current as a function of the spin-delocalization extent can be readily understood in terms of (i) the vibronic spectrum of the mixed-valence reduced species (see Figure 7b) and (ii) the Franck−Condon overlap factors (see

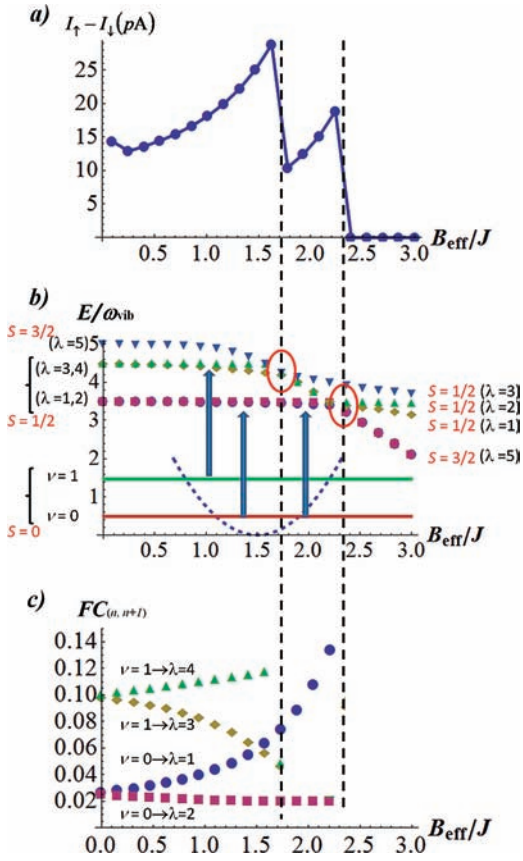

Figure 7. Spin-transport calculations for a weakly delocalized (Class I and Class II) mixed-valence Fe-dimer: (a) spin current as well as (b) oxidized and reduced lowest lying vibronic energy spectrum and (c) square of the overlap between oxidized and reduced vibronic wave function, all plotted as function of spin-delocalization B_{eff}/J. In part (b) the gap between the oxidized and the reduced manifolds of vibronic states is arbitrary and can be modulated via a gate voltage. The dashed black lines accross the three pictures indicate the values of B_{eff}/J for which level crossing (LC) occurs. The blue vertical arrows indicate the allowed pairs of charging processes: two pairs before the first LC, one pair between the first and second LC.

Figure 7c) between oxidized and reduced vibronic wave functions. In the weak delocalization regime, the ground and first excited vibronic states ($\lambda = 1$ and $\lambda = 2$) of the reduced species consist of two weakly split doublets (bonding and antibonding combinations of eq 6). The energy gap between the two doublets grows as function of B_{eff}/J, up to $\sim$7 cm^{-1} at the first discontinuity. The next excited vibronic states consist again of two weakly split doublets ($\lambda = 3$ and $\lambda = 4$), separated from the ground state by approximately one vibrational quantum. Thus, the four lowest lying vibronic states of the reduced mixed-valence system are all spin-angular momentum accessible from the singlet ground states in one-electron charging precesses. Furthermore, the energy gap between the ground ($\nu = 0$, $S = 0$) and first excited ($\nu = 1$, $S = 0$) vibronic states of the oxidized species is exactly $\hbar\omega_{vib}$, and thus the two states can both be brought simultaneously in resonance with the four lowest lying doublets of the reduced system, by a gate voltage of appropriate magnitude. Four different charging processes are responsible for sequential tunneling through the Fe(III)Fe(III) dimer: two from the $\nu = 0$ oxidized vibronic singlet to the $\lambda = 1$, 2 reduced doublet states and two from the first excited vibrational singlet state ($\nu = 1$) to the two reduced vibronic doublets $\lambda = 3$, 4 (see Figure 7b).

These four processes all require approximately the same energy; thus they will all contribute to spin transport. Since the harmonic oscillator functions of the oxidized and reduced species are displaced with respect to each other by $|\xi_-^A - \xi_0| = |\xi_-^B - \xi_0| = \lambda_-/2k_-$, Franck−Condon ($FC_{n, n+1}$) factors (i.e., square of overlaps between vibronic wave functions) will appear in the calculation of the transition rates reported in eqs 3 of the Supporting Information. The quantities $FC_{n, n+1}$ for the four contributing transitions are plotted in Figure 7c as a function of B_{eff}/J. It is evident from the plot that the overlap factors associated with the two transitions ($\nu = 0 \rightarrow \lambda = 1$ and $\nu = 1 \rightarrow \lambda = 4$) grow larger as a function of the double-exchange parameter, whereas the remaining two transition overlaps grow weaker with increasing spin delocalization. This behavior is consistent with the spin-delocalization process. For instance, the lowest mixed-valence doublet consists mainly of the symmetric mixing (bonding combination) of two displaced $\nu = 0$ functions. With increasing spin delocalization, vibrational excited states mix in, rapidly shifting the probability density of the two $\nu = 0$ functions toward the "bonding region", i.e. toward the center, where lies the probability maximum for the oxidized vibrational wave function $\nu = 0$. On the other hand, the antibonding combination starts off already with low density in the bonding region, and as B_{eff}/J grows larger, the excited states mix-in process only slowly pushes the probability density out of the central region, thus diminishing its overlap with the oxidized vibrational ground state. The fast growth of $FC_{n, n+1}$ for two of the dominant charging processes as a function of B_{eff} is of course a direct consequence of the decreasing depth of the double-well potential (see bottom of Figure 4) with increasing spin delocalization, and it explains the rapid increase of spin current *vs* B_{eff} observed in Figure 7a. Thus, for weak delocalization energy B_{eff}, mixed-valence dimers are found to behave as one would intuitively expect. However, this intuitive behavior can only be expected until the first spin transition occurs, after which the onset of the double-exchange blockade will rapidly quench charge and spin sequential tunneling transport.

Finally, the two discontinuities appearing at $B_{eff}/J \approx 1.7$ and $B_{eff}/J \approx 2.3$ are explained in terms of vibronic level crossings in the spectrum of the mixed-valence system (see Figure 7b; the vibronic level crossings are highlighted with red ovals). The first crossing occurs between a high-lying vibronic quartet ($S = 3/2$, $\lambda = 5$) and the excited doublets $\lambda = 3$ and $\lambda = 4$. A finer grid would actually show two different discontinuities, associated with the two different level crossings. The reason why the current drops after the level crossing is associated with a partial double-exchange blockade mechanism, in that two of the four accessible vibronic transitions are replaced, after crossing, by new *spin-forbidden* transitions $S = 0 \rightarrow S = 3/2$. However, after the first level crossing, two charging processes are still spin-allowed, and the current, although weaker, starts increasing again as a function of spin delocalization, by virtue of the Franck−Condon increasing overlap for the $\nu = 0 \rightarrow \lambda = 1$ process. At $B_{eff}/J \approx 2.3$, a second level crossing occurs, which changes the ground state of the mixed-valence species from a doublet to a quartet. After this second level crossing, the double-exchange spin blockade mechanism previously described is fully active, and no current is allowed to tunnel through the Fe(III)Fe(III) dimer.

According to our model, $[Fe_2S_2]^+$ mixed-valence complexes, Class II systems with a doublet ground state,[10] are predicted to be conductive in the sequential tunneling regime. On the other

hand, we predict the oxidized dimer of the $[Fe_2(OH)_3(tmtacn)_2]^{2+}$ Class III system[10] to be nonconductive, by virtue of the double-exchange blockade mechanism.

Conclusions

We have theoretically investigated molecular conductance through mixed valence binuclear complexes of types II and III. Quite counterintuitively, we find that the conductance in the sequential tunneling regime is blocked in type III complexes (characterized by a full delocalization of the excess electron) if the localized spins in the neutral complex (without excess electron) couple antiferromagnetically, which is usually the case. The ultimate reason for the blocking of the conductance in this case is the double-exchange mechanism, changing the lowest states from antiferromagnetic to ferromagnetic when an excess electron is added to the complex. The blocking mechanism can therefore be named double-exchange blockade. This is found in contrast to other mixed-valence compounds without core spins localized at the metal site, such as the Ru(II)Ru(III) mixed-valence Creutz−Taube complex,[7] where no such effect has been found in the conductance,[29] in agreement with the prediction of the model presented here based on simple spin-symmetry arguments (i.e., without an on-site magnetic core, the charging process always gives rise to a mixed-valence spin state with $S = 1/2$, no matter how strong the double-exchange delocalization is). On the other hand, in the complexes of types I and II the conductance is not quenched in the lower spin states and increases with increasing spin delocalization. We emphasize that the situation with the delocalization of an excess electron in *isolated* mixed-valent complexes is just the opposite: in the lowest states the excess electron is delocalized over two metal sites in class III complexes and is localized at one of the metal sites in class I and II compounds.

In the present work we focused on the sequential tunneling scenario arising from the application of the minimal value of a gate voltage providing an exact resonance between the lowest neutral and reduced states of the complex, for a fixed and low value of bias voltage. Varying gate and bias voltages will result in oscillations of the conductance as a function of the relative positions of vibronic levels localized at the two wells of the adiabatic potential of the complex. Although these additional details are necessary to simulate an experimental conductance spectrum for a Class I or II system, they do not affect the main conclusions drawn for Class III spin-delocalized systems. The experimental verification of the double-exchange spin blockade effects can be attained by measuring molecular conductance through binuclear mixed-valence complexes such as, e.g., $[Fe_2(OH)_3(tmtacn)_2]^{2+}$ and $[Fe_2S_2]^{+}$ complexes, using for instance the same experimental molecular break-junction setup, as already performed in similar transport investigations on magnetic molecules.[3−5] It would be sufficient to measure the conductance for low bias voltages close to the resonance between the neutral and lowest reduced states of the complex, for a range of mixed-valence systems characterized by a different extent of spin delocalization.

Acknowledgment. A.S. would like to thank the Flemish centre of excellence *Institute for Nanoscale Physics and Chemistry* (INPAC), at the K.U.Leuven, for financial support.

Supporting Information Available: Vibronic interaction matrix; Coulomb-blockade spin transport formalism. This material is available free of charge via the Internet at http://pubs.acs.org.

JA101887F

(29) Borshch, S. A.; Chibotaru, L. F.; Rousseau-Violet, J. *Chem. Phys.* **1998**, *229*, 223.